Maastricht University

Maastricht Science Programme
Faculty of Science and Engineering

Investigating CP-Violation in $B^{\pm} \to K^{\pm} K^{\pm} K^{\mp}$ Decay

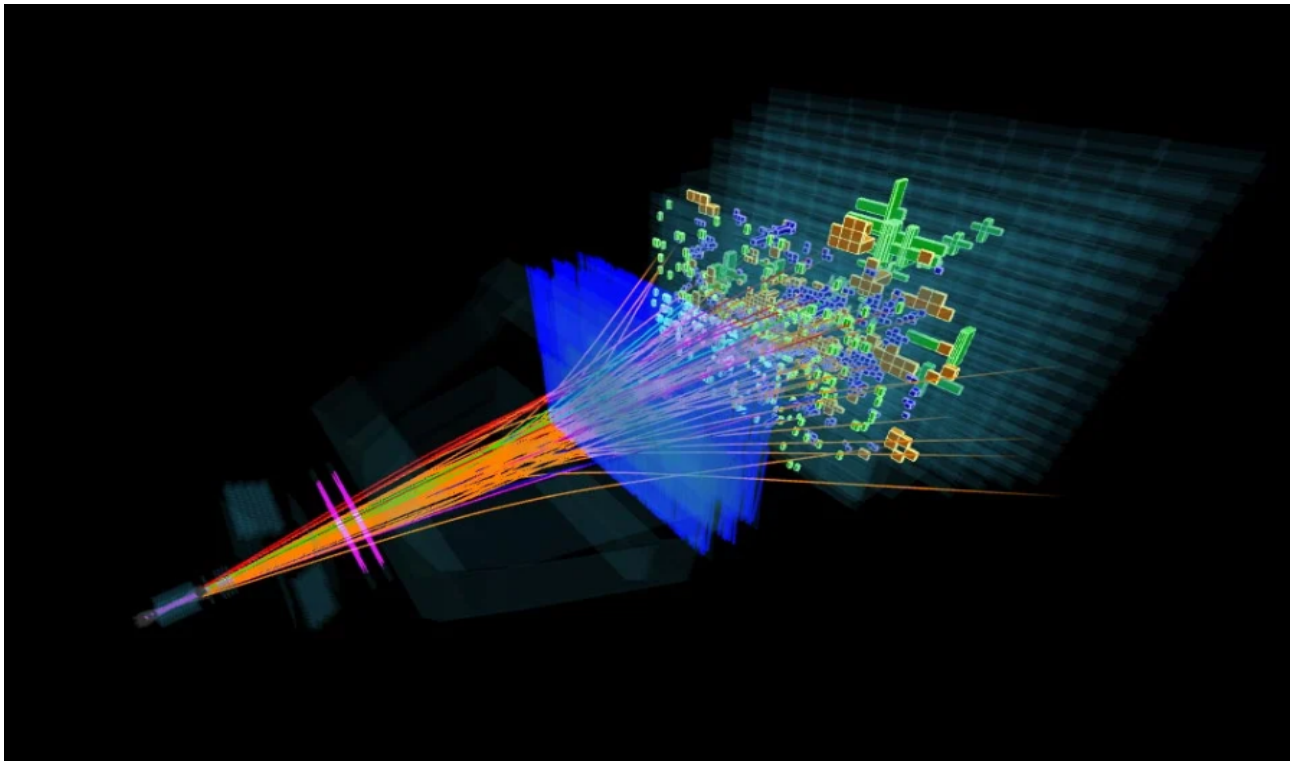

A typical LHCb event fully reconstructed during data taking on May 9th 2016. Particles identified as pions, kaon, etc. are shown in different colours [1].

Authors:

Brand, Oliver (i6302801)
Adaş, Defne (i6350415)
Gorzelany, Jakub (i6354860)
Hamers, Jenna (i6360895)
Ramirez, Regina (i6335493)
van Rosmalen, Nelson (i6324038)
Hamersma, Finn (i6309146)

Supervisors:

Keri Vos, Marta Burgos Marcos, Joan Ruiz Vidal

Academic Year:

2024-2025

Word Count:

1 Abstract

This project investigates the violation of CP symmetry in the decay processes of $B^{\pm} \to K^{\pm}K^{\pm}K^{\pm}$, utilizing open data collected by the LHCb experiment in 2011. These specific decays were chosen due to the rich kinematics that are inherent to three-body decays, which make them very sensitive to CP-violating effects. The analysis conducted in this study involved calculating the invariant mass of neutral kaon pairs to construct Dalitz plots, from which 1D projections could be made. Using the peaks present in those it was possible to identify several resonances by comparing the obtained mass distributions to data from the Particle Data Group (PDG). These Dalitz plots could be constructed from the dataset, which was previously selected based on criteria such as momentum, reconstructed mass from decay products, and impact parameters. Background noise was filtered out using a probability density function (PDF) fitted to the mass distribution plots. A statistically significant CP asymmetry was found for the $B^{\pm} \to K^{\pm}K^{\pm}K^{\mp}$ decay. The findings of this research contribute to the broader effort of understanding CP violation and its implications for the Standard Model (SM) of particle physics. The observed CP asymmetry can provide a better understanding of the workings of the Standard model, and potentially indicate new physics beyond.

Table of Contents

Contents

List of Figures

List of Tables

2 Introduction

The Standard Model is the fundamental framework describing the particles and forces that govern our universe. The model consists of six quarks and six leptons that are divided into three generations with increasing mass. Almost all matter in the universe consists of the lightest up- and down-quarks, while the heavier charm, strange, top, and bottom quarks, occur only in high-energy environments. Though the SM is considered the most successful scientific theory, it requires further refinement and expansion as some phenomena can not be explained within the framework. One such phenomenon is the dominance of matter over antimatter in the universe, which suggests the need for physics beyond the SM [2].

To explain this matter-antimatter asymmetry, Sakharov proposed three conditions as necessary criteria for generating a matter-dominated universe [3]. One of these conditions is charge-parity (CP) symmetry violation. An amount of CP violation can be accounted for within the SM, through the weak force. However, this amount of CP violation is not enough to explain the observed matter-antimatter asymmetry. This conflict is investigated using the Large Hadron Collider at CERN in the LHCb experiment. There, the high-energy environments necessary for generating high-energy particles are obtained by accelerating and colliding particles. This project used an open data set from an LHC run in 2011 provided by the LHCb experiment [4] which contains various $B^{\pm}$ three-body decays. B-mesons decay in many different ways, allowing opportunities to explore new physics via various kinematic structures. Through investigation of CP violation in three-body B-meson decays, this study contributes to ongoing efforts to understand and account for the observed matter-antimatter asymmetry. In the future, modern theoretical models can then be examined and expanded by comparing our experimental results with predictions based on the SM.

This study aimed to determine the CP violation in the LHCb open data by comparing the decay rate of B-mesons (B^+) with the decay rate of their antiparticles (B^-) to gain more insight into the workings of the weak force and its CP violation.

3 Theory

3.1 Standard Model

The standard model describes the smallest observed building blocks of reality. It consists of three groups, namely quarks, leptons, and bosons. Quarks are the constituents of Hadrons and consist of six flavours: up and down(I), charm and strange(II), and top and bottom(III). Leptons include the electron(I), muon(II), and tau(III) particles with their corresponding neutrinos. The 4 vector bosons act as force carriers mediating the weak, strong, and electromagnetic interactions. The fifth, scalar boson is the Higgs boson, which is understood to give particles their mass [5].
The weak force is particularly relevant in this paper, as it is the only fundamental force known to act differently for particles and their antiparticles, thereby violating CP-symmetry [5].

3.2 CP-symmetry, CKM matrix

Charge conjugation symmetry implies that nature treats matter and antimatter the same way. Charge conjugation (C) converts each particle into its antiparticle, which changes all internal quantum numbers such as charge and baryon numbers but mass, energy, momentum, and spin remain the same [6].
Meanwhile, parity symmetry suggests that the fundamental interactions occur identically for particles and their counterparts with spatially inverted coordinates. In other words, a mirrored particle behaves the same as the original. Together, these operations result in a discrete gauge symmetry that remains unchanged for most particles. Charge parity (CP) symmetry implies that flipping the quantum numbers together with left or right-handedness of particles will not alter how the fundamental forces interact with them. CP symmetry is conserved by both the electromagnetic and the strong force, but violated by certain interactions with the weak force [7]. Weak interactions are not invariant under the parity transformation P, nor the charge conjugation C, as it was observed that some weak interactions with matter occur more frequently than with antimatter [6].
The CPT symmetry was proposed in the 1950s as a true symmetry of nature, to account for the violation of separate C, P, and T (time) symmetries. The CPT symmetry theorem states that the combined operation of time reversal, charge conjugation, and parity (in any order) is an exact symmetry of any interaction [8].
The violation of CP symmetry permits different outcomes for the same events involving particles and their

antiparticle counterparts. This phenomenon is a key contributor to the dominance of matter over antimatter in the universe [9].
As mentioned above, CP symmetry violation in the theoretical framework lies in weak interactions, which are responsible for mediating flavour changes via $W^{\pm}$ bosons. The amplitudes of these flavour-changing interactions differ between generations and are encoded by the Cabbibo-Kobayashi-Maskawa (CKM) mechanism in the CKM matrix. The standard parametrization of the CKM matrix with $s_{ij} = sin(\theta_{ij})$, and $c_{ij} = cos(\theta_{ij})$ can be expressed as

$$V_{CKM} = \begin{pmatrix} V_{ud} & V_{us} & V_{ub} \\ V_{cd} & V_{cs} & V_{cb} \\ V_{td} & V_{ts} & V_{tb} \end{pmatrix} = \begin{pmatrix} s_{12}c_{13} & s_{12}c_{13} & s_{13}e^{-i\delta_{13}} \\ -s_{12}c_{23} - c_{12}s_{23}s_{13}e^{i\delta_{13}} & -c_{12}c_{23} - s_{12}s_{23}s_{13}e^{i\delta_{13}} & s_{23}c_{13} \\ -s_{12}c_{23} - c_{12}s_{23}s_{13}e^{i\delta_{13}} & -c_{12}c_{23} - s_{12}s_{23}s_{13}e^{i\delta_{13}} & s_{23}c_{13} \end{pmatrix} \quad (1)$$

where V_{CKM} is a complex 3x3 matrix. Due to the unitarity conditions and symmetries in the standard model, the 18 possible real independent parameters are reduced to 4. These are three mixing angles $(\theta_{12}, \theta_{13}, \theta_{23})$ describing the mixing between families, and a phase δ. The phase is the only source of CP violation in the standard model [10]. The CKM matrix encodes the amplitude for each possible flavour change as V_{ij}, e.g. a strange quark changing into an up quark is described by V_{us}. The values encoded are only valid for a down-type quark or antiquark decaying. For up-type quarks or antiquarks decaying, e.g. an up quark becomes a strange quark, the amplitude is displayed as $V_{us}^{\star}$ and is the complex conjugate of the initial amplitude. Furthermore, the two applications of taking the complex conjugate cancel each other out where, for example, an anti-strange decaying into an anti-up would follow $V_{us}^{\star}$, while an anti-up becoming an anti-strange would be described by V_{us}. The matrix is used to calculate the Jarlskog invariant which provides a measure for the amount of CP violation expected from nature. The resulting value $(J = 3 * 10^{-5})$ is too small to account for the dominance of matter over antimatter, and as mentioned earlier, suggests physics beyond the standard model [11].

3.3 CP violation in $B^{\pm} \to K^{\pm}K^{\pm}K^{\mp}$ decay

The decay of $B^{\pm} \to K^{\pm}K^{\pm}K^{\mp}$ is quite rare and can occur via multiple pathways, one of those is represented by the Feynman diagram shown in Figure 1.

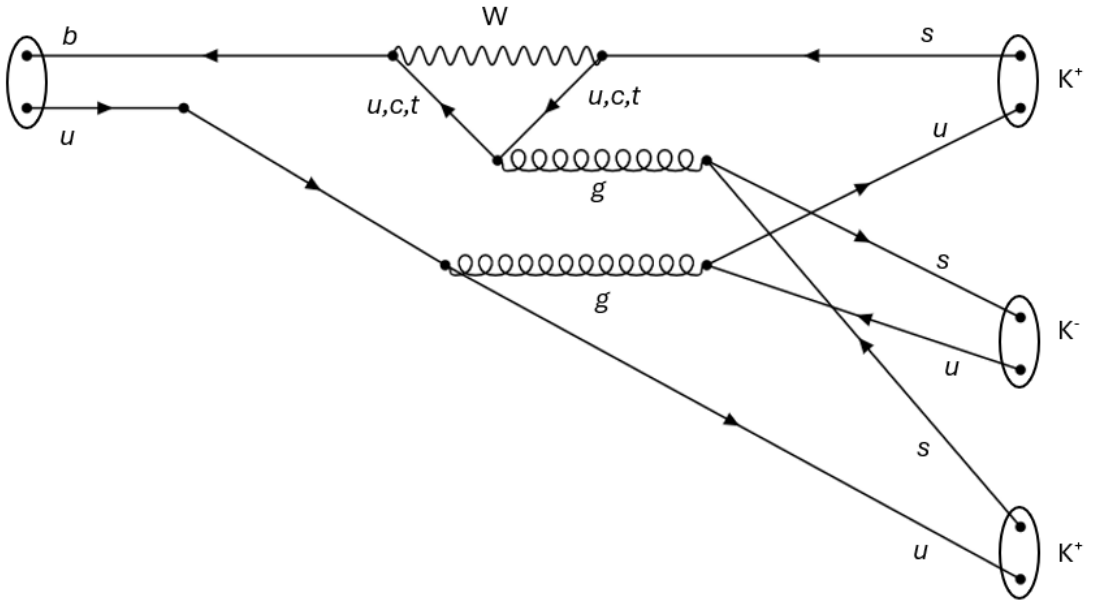

Figure 1: Feynman diagram of $B \to K^{\pm}K^{\pm}K^{\mp}$ decay

This structure is known as the penguin diagram, which refers to the upper decay containing the loop. The given pathway is an example of a direct decay where the B meson decays directly into the three Kaons. The decay can also occur with an intermediate structure called a resonance, and this is depicted as $B^{\pm} \to K^{\pm}R$ where R later decays as $R \to K^{\pm}K^{\mp}$. An example of the decay with J/ψ resonance is depicted in Figure 2.

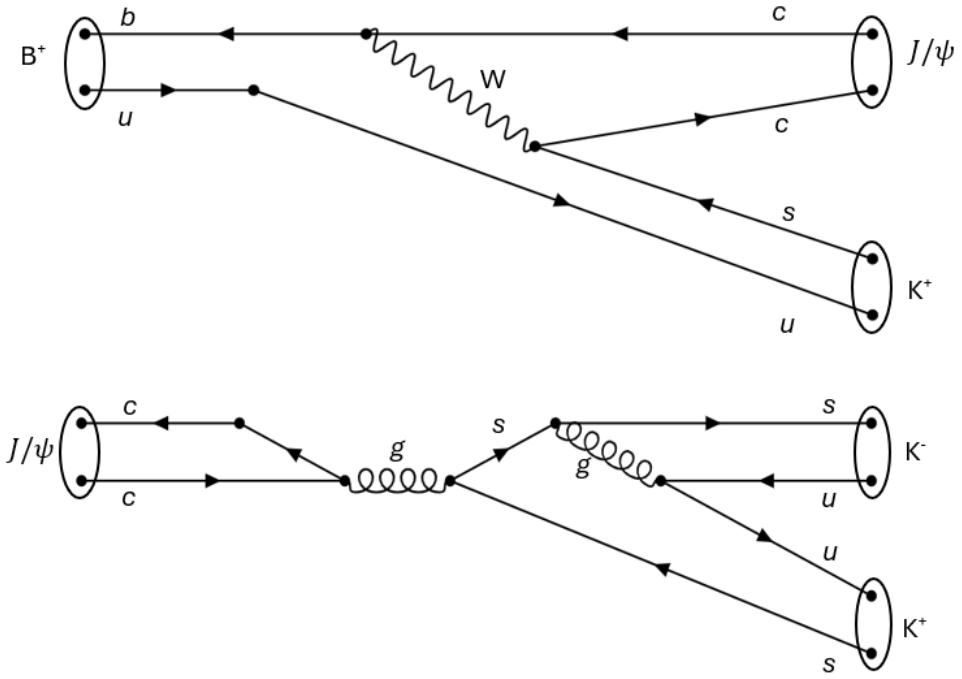

Figure 2: Feynman diagrams of $B \to K^+ J/\psi$ and $J/\psi \to K^+K^-$ decay

Regardless of the pathway through which it decays, all $B^{\pm} \to K^{\pm}K^{\pm}K^{\mp}$ decays contain at least 1 weak interaction. This can be concluded from the fact that the B^+ meson consists of 1 up quark and 1 anti-bottom quark, while the kaons consist of (anti-)up quarks and (anti-)strange quarks. This shows a flavour change happened, which can only occur via a $W^{\pm}$ boson. From the CKM matrix in Equation 1 it can be deduced that all three pathways of b quark into s quark decay, namely $b \to t \to s$, $b \to c \to s$ and $b \to u \to s$, with the amplitudes $V_{tb}V_{ts}^*$, $V_{cb}V_{cs}^*$ and $V_{ub}V_{us}^*$ respectively, all contain a complex phase δ that is responsible for CP violation.

To quantify this CP violation, the CP asymmetry, defined by

$$A_{CP} = \frac{\Gamma(B^- \to K^+K^+K^-) - \Gamma(B^+ \to K^-K^-K^+)}{\Gamma(B^+ \to K^+K^+K^-) + \Gamma(B^- \to K^-K^-K^+)}, \tag{2}$$

can be calculated, where Γ is the decay rate of both $B^{\pm}$. This is the probability per unit time that a given particle will decay. Moreover, it is closely related to the decay amplitude, which is the probability of the decay into a certain final state [12] as

$$\Gamma \propto |A|^2. \tag{3}$$

When a weak decay channel receives contributions from two coherent processes, the total decay amplitude is the sum of the transition amplitudes

$$A(B^+ \to K^+K^+K^-) = A_1 e^{i\delta_1} e^{i\phi_1} + A_2 e^{i\delta_2} e^{i\phi_2} \tag{4}$$

where $\phi_{1,2}$ are phases due to the weak decay dynamics and $\delta_{1,2}$ are due to strong (or electromagnetic) final-state interactions [13]. For the CP conjugate amplitude, the expression is

$$\bar{A}(B^- \to K^-K^-K^+) = A_1 e^{i\delta_1} e^{-i\phi_1} + A_2 e^{i\delta_2} e^{-i\phi_2} \tag{5}$$

By combining Equation 2 with Equation 3 and plugging into Equation 4 and Equation 5, the CP asymmetry formula, with respect to phase and amplitude, is obtained:

$$A_{CP} = \frac{2|A_1||A_2|\sin(\delta_1 - \delta_2)\sin(\phi_1 - \phi_2)}{|A_1|^2 + |A_2|^2 + 2|A_1||A_2|\cos(\delta_1 - \delta_2)\cos(\phi_1 - \phi_2)} \tag{6}$$

For CP violation to occur, Equation 6 must be non-zero. This condition is satisfied if both the particle and antiparticle decay amplitudes are non-zero, and if there is a non-zero difference between their weak and strong phases.
In principle, these three variables are all the necessary components to calculate the CP asymmetry within the framework of the Standard Model, yet accurately describing them has remained challenging. Like the amplitude, The weak phase arises from the CKM matrix, while the strong phase difference originates from complex hadronic strong interaction effects.
These strong interaction influences represent a major challenge for theoretical analyses due to long-distance effects, which cannot be analysed in perturbation theory [14]. Accurately describing these effects remains highly challenging, particularly when multiple intermediate resonances contribute to the process.

3.4 Invariant Mass and Resonances

In particle physics the mass is not conserved in most interactions except in elastic collisions [6], where the total kinetic energy and rest mass remain unchanged. This apparent loss or gain of mass in inelastic processes reflects the deeper principle that mass and energy are intrinsically interconnected, forming components of a unified four-vector:

$$P^{\mu} = \begin{pmatrix} E \\ p_x \\ p_y \\ p_z \end{pmatrix} = \begin{pmatrix} E \\ \vec{p} \end{pmatrix} \tag{7}$$

Its energy (E) and momentum vector (p_i), as measured in any other frame, can be combined to find the invariant ma, which means it does not change under coordinate transformations. [15] [16]

$$m^2 = E^2 - |\vec{p}|^2 = P^{\mu}P_{\mu} \tag{8}$$

The introduction of energy and momentum as components of a four-vector in relativistic mechanics becomes indispensable, as they enable precise calculations in high-energy physics where particles interact and transform. In both relativity and classical mechanics, collisions offer the clearest framework for applying these conservation laws effectively. [6] They illustrate how energy and momentum redistribution govern the behaviour of particles during the collision, revealing underlying symmetries and conservation principles that are widely researched in modern physics.

Resonances are instrumental in the detection of CP violation and show up as intermediate particles as a result of interactions between the two final-state particles of a decay. These particles exist for very short periods, often only on the order of 10^{-23} s. We can only detect them by inferring their existence from their decay products using an invariant mass distribution, where they appear as peaks for certain mass values. The invariant mass of a particle can be found using Equation 8.

Resonances are evident when the invariant mass of a pair of particles resembles that of an intermediate state. Examples of such intermediate states are those of vector mesons or scalar mesons. If a resonance has such a mass, it enhances the decay rate in the corresponding regions of the invariant mass distribution, which can be observed in Dalitz plots as a band or a peak.

3.5 Dalitz Plots

Dalitz plots are commonly used to give a graphical representation of the kinematics of three-body decays. Understanding how to read and interpret these graphs is essential for studying decay dynamics, identifying resonances, and visually identifying deeper aspects of particle interactions.
The axes of a Dalitz plot are the squared invariant masses of neutral particle pairs resulting from a three-body decay. Squared masses ensure that the axes are linear and nonnegative, which simplifies interpretation and makes the plot more intuitive [4].

The boundaries of the Dalitz plot are defined by the kinematics of the decay, specifically dictated by the energy and momentum conservation principle. The sum of the kinetic and rest energies of the decay products must equal the total energy of the decaying particle. This conservation gives as a result a plot with either a triangular

or curved form, within which all points must fall. The specific shape of the boundaries, or the figure of the plot, will depend on the masses of its decay products. The limits can be written as follows:

$$(m_i{}^2 + m_j)^2 \leq m_{ij}{}^2 \leq (M - m_k)^2 \tag{9}$$

where m_i, m_j and m_k are the invariant masses of the decay products in a three-body decay, $m_{ij} = m_i + m_j$ and M is the invariant mass of the decaying particle.
Once mentioned the components and limitations used to construct and interpret a Dalitz plots, we can expect to observe a figure similar to:

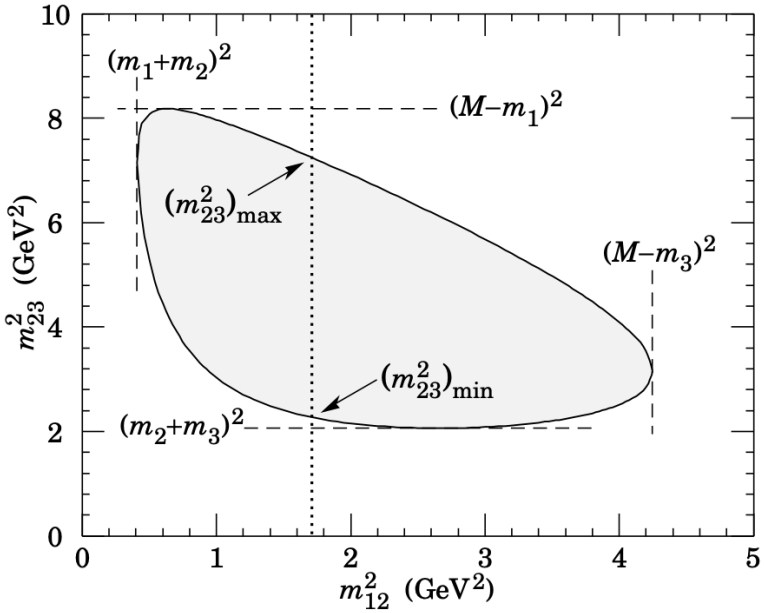

Figure 3: Dalitz plot for a three-body final state
[17]

Where as mentioned previously, Four-momentum conservation restricts events to the shaded region and the axis are the invariant squared masses of the final-state particles.

In the Dalitz plot, dense areas indicate resonance structures or preferred decay pathways within the plotted data, while empty bands signify resonance structures that were excluded from the sample.
Resonances can be identified through several shapes in the plot. They might appear as bands or arcs, corresponding to the squared invariant mass of a particle pair near the mass of the intermediate state. A vertical band could indicate a resonance in one pair system, while a diagonal feature might reflect a resonance involving one particle and the combined mass of the other two. Interference effects between overlapping resonances can create more complex patterns, such as ripples or modulations in the density distribution.

Symmetry or asymmetry in the Dalitz plot can also provide insight into the underlying physics. When two of the decay products are identical particles, such as in the analyzed decay $B^{\pm} \to K^{\pm}+ K^{\pm}+ K^{\mp}$, the Dalitz plot will exhibit a reflection symmetry about the diagonal. Deviations from such symmetry, or asymmetrical density distributions, can point to phenomena such as CP violation.

Interpreting a Dalitz plot involves distinguishing the signal from the background. Uniform distributions or low-density regions may indicate background noise, while clear structures and patterns are typically associated with the physical processes of interest. The boundaries of the plot itself can yield information about threshold effects, where the onset of a resonance structure might create a sharp increase in density near the edge of the kinematic region.
In the decay $B^{\pm} \to K^{\pm}+ K^{\pm}+ K^{\mp}$, a Dalitz plot might reveal a vertical band corresponding to the formation of a $K^{\pm}+ K^{\mp}$ system. The symmetry of the plot reflects the indistinguishability of the two $K^{\pm}$ particles, and the

density variations can aid in identifying interference effects or other dynamic features of the decay. Similarly, in the decay, $D^0 \to K^+ + K^- + \pi^0$, the appearance of a ϕ resonance in the K^+K^- system would manifest as a narrow band around the mass of the ϕ [18].
In addition to identifying decay products and resonance structure Dalitz plots are used to analyse the nature of intermediate states, and the intricacies of quantum interference.

4 Methodology

For the investigation of CP-symmetry violation, a set of pre-cut B-meson decay data from LHCb open data was used [4]. The pre-selection of this data was based on three criteria: the momentum of the final mesons, the reconstructed mass of the B-meson from its decay products, and the impact parameter, which demonstrates statistical significance at higher values. Using these criteria, the data was pre-selected for $B^{\pm} \to h^{\pm} + h^{\pm} + h^{\mp}$ decay with $h = \pi, K$ and stored in a ROOT-file. The table below shows the variables present in the ROOT-file for each of the three charged particle tracks H1-H3.

Table 1: Overview of the variables in the pre-selected data set for the charged particle track 1 (H1)

Variable	**Description**
H1 PX	Reconstructed momentum component of particle in X direction [MeV/c].
H1 PY	Reconstructed momentum component of particle in Y direction [MeV/c].
H1 PZ	Reconstructed momentum component of particle in Z direction [MeV/c].
H1 ProbK	Likelihood of particle being Kaon [range 0 to 1].
H1 ProbPi	Likelihood of particle being Pion [range 0 to 1].
H1 Charge	Particle charge (+1 or -1).
H1 isMuon	Identification of track as a muon, obtained from muon chamber hits (0 is false, 1 is true).
B FlightDistance	The distance travelled by the B candidate before decaying. Obtained from the distance from the primary vertex to the vertex made by three charged tracks [mm].
B VertexChi2	χ^2 of the quality of the vertex made by the three charged tracks.
H1 IPChi2	Impact Parameter χ^2.

The processing of this pre-cut data and creation of the plots mentioned was done using code written in Python specified in Appendix A and using Uproot.
As is visible in Table 1 the pre-cut set of data still included tracks that corresponded to pions and muons, so the first cut that was performed was removing all interactions that contained tracks with a probability of being a kaon below 60%, as well as removing all interactions that contained a track that was identified as a muon. After making sure the data contained only the tracks corresponding to kaons, the invariant mass of the supposed $B^{\pm}$ was reconstructed from the kaon tracks using an adapted version of Equation 8. For this specific case E is the combined energy of the three kaons

$$E = \sqrt{m^2 + p_{x,123}^2 + p_{y,123}^2 + p_{z,123}^2} \tag{10}$$

and $\vec{p}$ is the combined momentum vector of the three kaons:

$$\vec{p} = \begin{pmatrix} p_{x,123} \\ p_{y,123} \\ p_{z,123} \end{pmatrix} = \begin{pmatrix} p_{x1} + p_{x2} + p_{x3} \\ p_{y1} + p_{y2} + p_{y3} \\ p_{z1} + p_{z2} + p_{z3} \end{pmatrix} \tag{11}$$

The results were plotted into a frequency-mass graph, after which a cut was made to exclude data that did not yield a mass close to the theoretical mass of the B meson. The invariant masses of the neutral two body combinations, $m(K^+K^-_{low})$ $m(K^+K^-_{high})$, were calculated based on the remaining event data and squared to enable the consbvbtruction of the Dalitz plot. This was then also split into the B^+ and B^- events. Projections of the Dalitz plots onto the x-axis were created as well to highlight potential resonances. These projections, compared with information from the Particle Data Group (PDG) listings, allowed the identification of significant peaks that correspond to the intermediate particles.
From the complete data of the invariant $B^{\pm}$ mass, the mass for the B^+ and B^- were extracted, which were plotted in a frequency-mass plot. By fitting a function to each graph, the background could be removed while

simultaneously obtaining a function that could be integrated to obtain accurate event counts. This step was critical to obtaining reliable values for the CP asymmetry.
Since the detection period for both the B^+ and B^- decays are the same Equation 2 was rearranged into

$$A_{CP} = \frac{N^- - N^+}{N^+ + N^-} \tag{12}$$

where CP asymmetry was then determined by comparing the observed number of events for positively and negatively charged B mesons.
Here, A_{CP} is the CP asymmetry, N^+ the number of events from the decay of B^+ in the considered channel, and N^- the number of events from the decay of B^- in the same channel. Using the error values provided along the curve fit, error propagation was performed to provide the most accurate amount of CP violation. Using Equation 12 and the error propagation, the CP asymmetry found was compared with the LHCb result.

5 Results & Discussion

5.1 Event reconstruction & B meson selection

Having rid the data of the events containing muon and pion tracks as mentioned before, the invariant mass of the B-meson was calculated as mentioned in Equation 8 and Equation 7 and plotted as a histogram of frequency against mass, as shown in below in Figure 4. The expected mass of the B meson is 5279.41 ± 0.07 MeV according to PDGlive [19]. The data in the figure was cut so there are at least 50 entries for a given MeV value for the plots and calculations below. This resulted in a selection of reconstructed B mesons with their reconstructed invariant masses in the range [5252, 5315] MeV. It should be noted that this cut was not applied while determining the global CP violation.

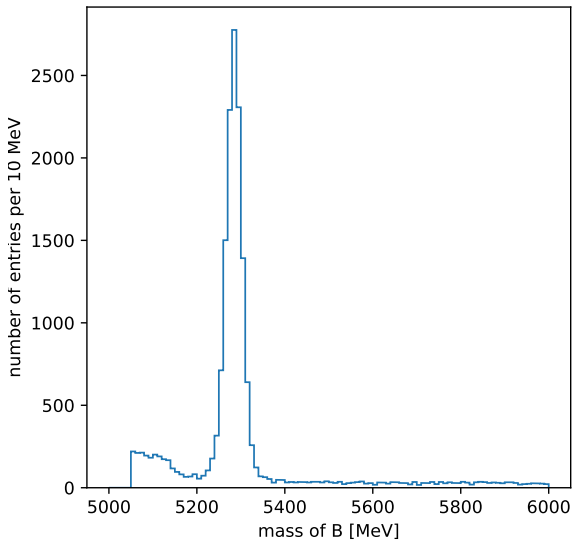

Figure 4: Distribution of invariant mass for the reconstructed B mesons

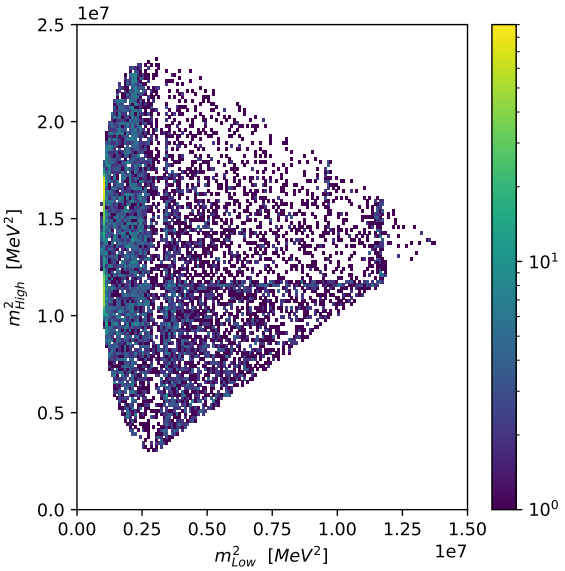

Figure 5: Dalitz plot of the number of $B^{\pm}$ mesons

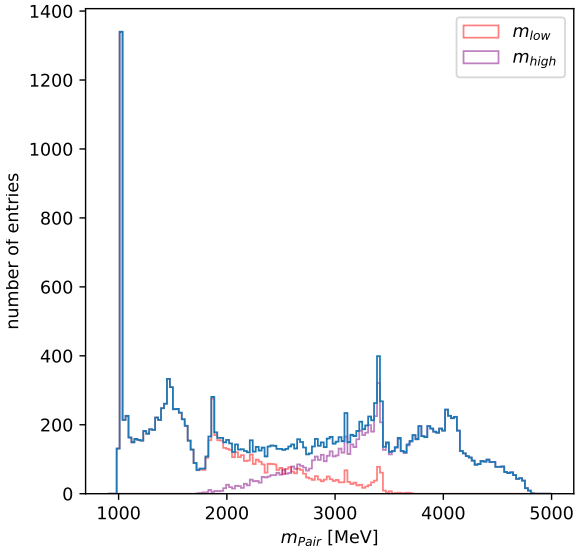

Figure 6: One-dimensional projections of the Dalitz plot on m_{low} and m_{high} axes

The Dalitz plot obtained from the cut data is shown in Figure 5, where the decay entries are plotted against the combined invariant masses of the K^+K^- pairs. To better investigate the structures seen on this plot, the 2-dimensional histogram was projected onto both axes to create one-dimensional histograms. The axis was changed from MeV^2 to MeV to obtain a direct reading of the mass values. Figure 6 shows these two histograms, but more importantly also shows their sum, which creates a continuous distribution of K^+K^- masses. This combined histogram was used to determine all possible resonance structures observed in $B^{\pm} \to K^{\pm}K^{\mp}K^{\pm}$. These possible resonances can be found in Table 2. Furthermore, the apparent vertical white line in the Dalitz plot corresponds to the lowest drop in Figure 6, this drop is suspected to be the influence of D^0 Mass - 1864.84 ± 0.05 MeV which decays into pions and was thus indirectly excluded from the data.

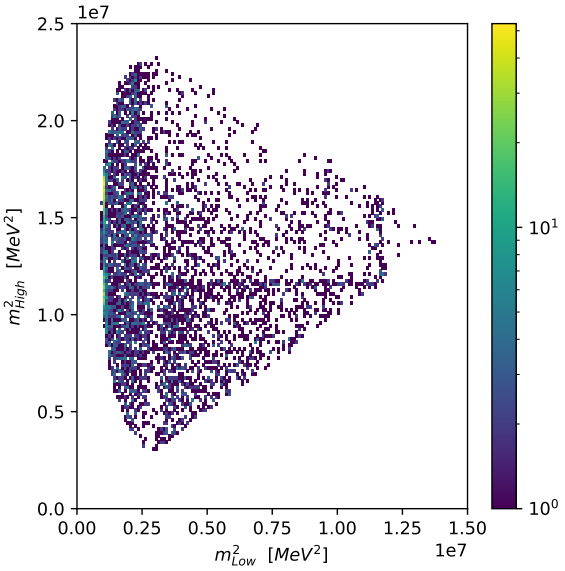

Figure 7: Dalitz plot for B^+ mesons

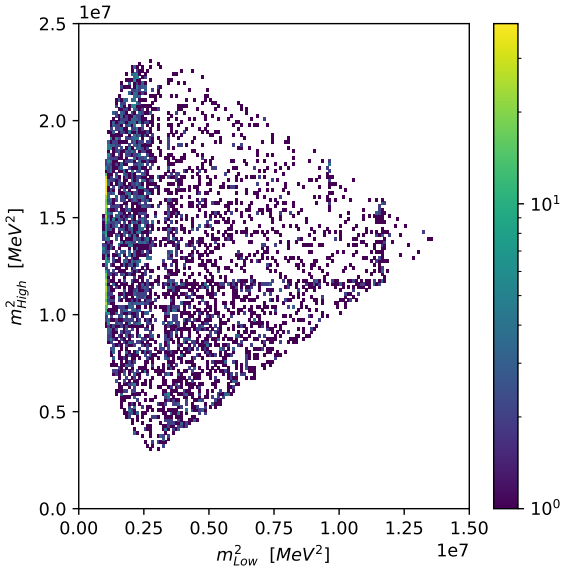

Figure 8: Dalitz plot for B^- mesons

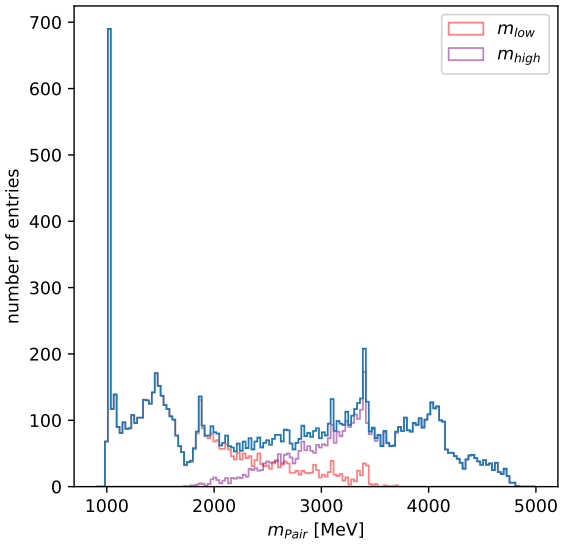

Figure 9: One-dimensional projections of the Dalitz plot for B^+ mesons on m_{low} and m_{high} axes

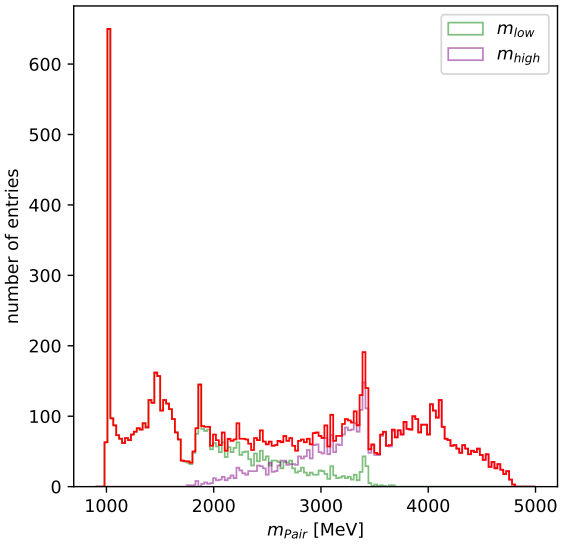

Figure 10: One-dimensional projections of the Dalitz plot for B^- mesons on m_{low} and m_{high} axes

Figure 7 and Figure 8 are the Dalitz plots for B^+ and B^- mesons separately, following the same convention as Figure 5 in axes. These two Dalitz plots show no visible difference in the distribution of the decays at this level. However, the projections given as Figure 9 and Figure 10 do show that there are fewer $B^- \to K^-K^-K^{-+}$ decays than B^+ decays in the analysed data set. The absence of unique identifiable structures indicates that the resonances in this decay do not depend on the charge.
To gain more insight into the meaning of the different peaks present in the one-dimensional projections of both the B^+ and B^-, PDG-live was used to find resonances with a mass in the $900 - 5000$ MeV range that could decay into a K^+K^- pair [19]. The results are visible in Table 2 below.

Table 2: Overview of all possible resonance structures in $B^{\pm} \to K^{\pm}K^{\pm}K^{\mp}$ decay

Resonance structure	I^G	J^{PC}	**Mass (MeV)**	**Width (MeV)**
$a_0(980)$	1^-	0^{++}	980 ± 20	$50 - 100$
$f_0(980)$	0^+	0^{++}	990 ± 20	$10 - 100$
$\phi(1020)$	0^-	1^{--}	1019.461 ± 0.016	4.249 ± 0.013
$a_2(1320)$	1^-	2^{++}	1318.2 ± 0.6	107 ± 5
$f_0(1370)$	0^+	0^{++}	$1200 - 1500$	$200 - 500$
$a_0(1450)$	1^-	0^{++}	1439 ± 34	258 ± 14
$\rho(1450)$	1^+	1^{--}	1465 ± 25	400 ± 60
$f_2(1810)$	0^+	2^{++}	1815 ± 12	197 ± 22
$f_2(1910)$	0^+	2^{++}	1941 ± 18	120 ± 40
$J/\psi(1S)$	0^-	1^{--}	3096.900 ± 0.006	$(92.6 \pm 1.7) \cdot 10^{-3}$
$\chi_{c0}(1P)$	0^+	0^{++}	3414.71 ± 0.30	10.7 ± 0.6
$\Psi(4160)$	0^-	1^{--}	4191 ± 5	69 ± 10

The column I^G depicts the quantum number I Isospin with G representing its property under G-parity, which is charge conjugation as well as a 180° rotation around the second axis of isospin space. The column J^{PC} stands for the angular momentum J with P representing its property under parity transformation and C is property under charge conjugation. While these numbers are not of great importance to the current analysis, they are essential for identifying these particles in the future based on an amplitude analysis that allows for the identification of resonances. The masses and widths shown in the table are the averages of the values collected from a multitude of data collection runs completed at multiple research sites. By examining the positions and widths of the peaks visible in Figure 6, each peak could be assigned a resonance that would explain their

appearance. The results are visible in Figure 11.

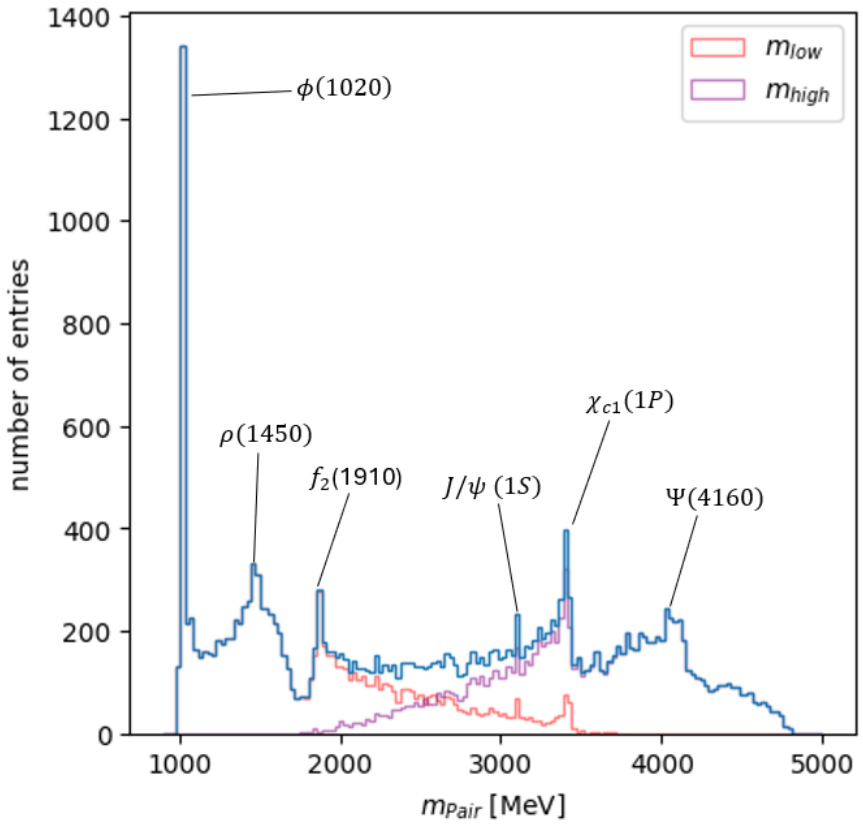

Figure 11: One-dimensional projection of the total Dalitzplot with labelled peaks

While the given plots are useful for gaining insight into the decay kinematics, the detector's background signal introduces inaccuracies in identifying the number of decays. To get an accurate reading for the number of decays, a best-fit line was used to differentiate between the background and detected mass of the $B^{\pm}$ mesons. The $B^{\pm}$ mass distribution is a Gaussian curve and the background signal was approximated to be linear. The initial cut based on the reconstructed $B^{\pm}$ mass was removed for the modelling and the obtained curve is described as

$$f(x) = Ae^{-\frac{(x-\mu)^2}{2\sigma^2}} + Bx + C \tag{13}$$

where A, B, C, μ, and σ are parameters obtained from the fit conducted via the code in Appendix A. The lower and upper boundaries of the fits were set to 5150 MeV and 5370 MeV respectively. These fit parameters are presented with their uncertainties in Table 3, and the plots are given in Figure 12 and Figure 13. The goodness of fits was tested with the code as well, where with 22 degrees of freedom $\chi^2 = 44.67$, $p < .005$ for the B^+ fit and $\chi^2 = 39.23$, $p < .025$ for the B^- fit.

Table 3: Parameters for the $B^{\pm}$ Mass Distribution Fits

Parameters (B^+)	**Value**	**Uncertainty**
μ (MeV)	5284.7660	0.1791
σ (MeV)	17.2434	0.2003
A (entries)	1393.2665	12.8615
B (entries/MeV)	-0.0516	0.0637
C (entries)	312.7849	333.9235
Parameters (B^-)	**Value**	**Uncertainty**
μ (MeV)	5284.4539	0.1611
σ (MeV)	17.6628	0.1807
A (entries)	1260.9583	10.2216
B (entries/MeV)	-0.0481	0.0513
C (entries)	288.8684	268.8030

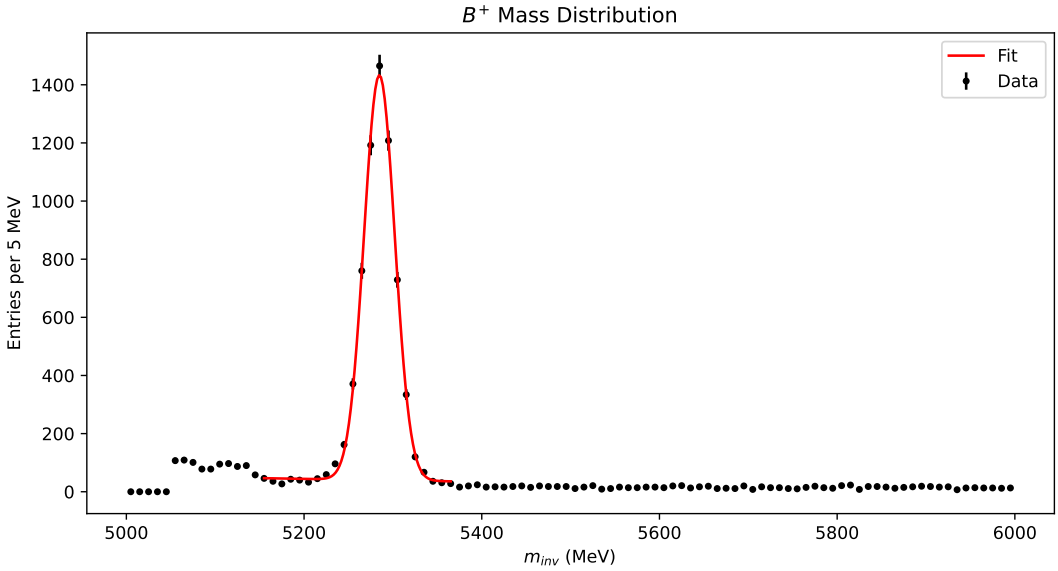

Figure 12: Best fit line over the uncut reconstructed B^+ mass

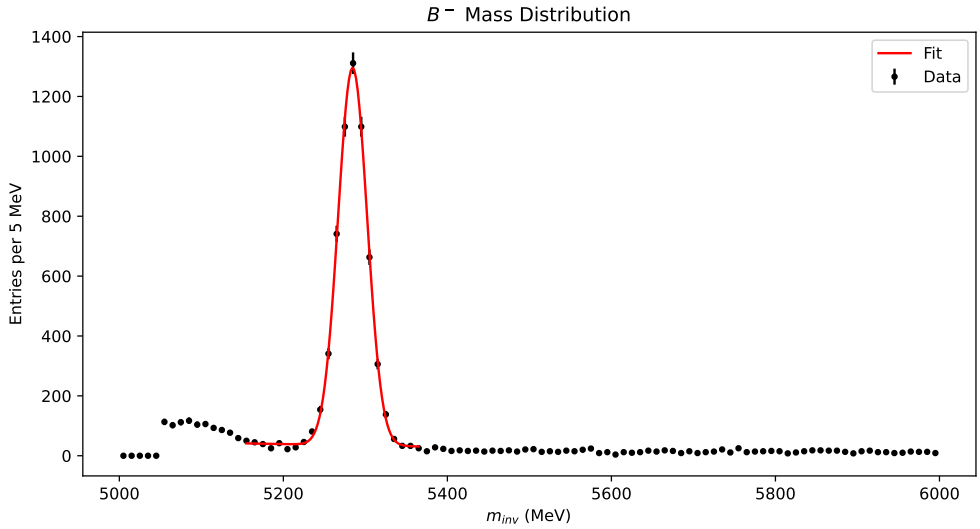

Figure 13: Best fit line over the uncut reconstructed B^- mass

The Gaussian distribution obtained from the fit was integrated to obtain the total number of $B^{\pm}$ decays as

$$N^{\pm} = A\sigma\sqrt{2\pi} \tag{14}$$

where $N^+ = 6019 \pm 894$ and $N^- = 5583 \pm 729$. Therefore the global CP asymmetry calculated according to Equation 12 is

$$A_{CP} = \frac{5583 \pm 729 - 6019 \pm 894}{5583 \pm 729 + 6019 \pm 894} = -0.0379 \pm 0.0099 \tag{15}$$

This value is very similar to the results published by LHCb, where some difference is expected since the referenced report draws data from multiple runs [20].

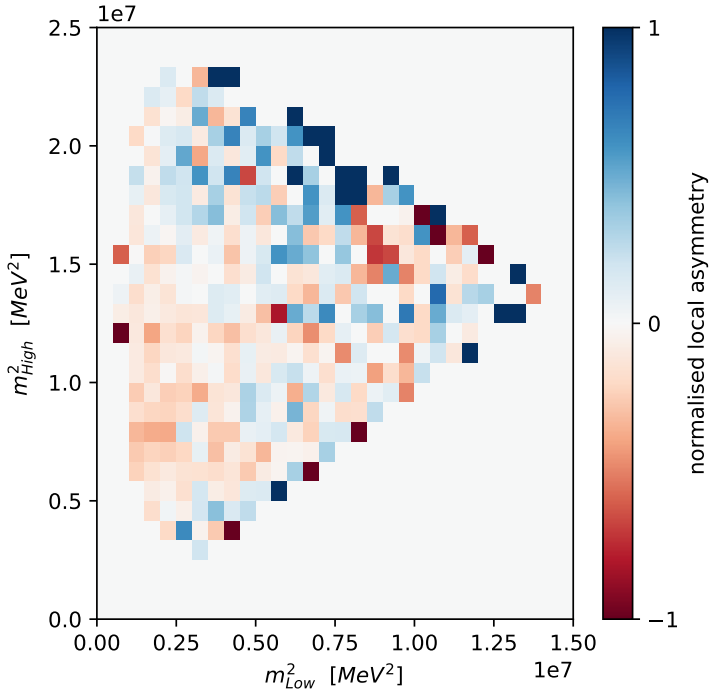

Figure 14: Normalized difference between Dalitz plots

Figure 14 shows the normalised difference between the two Dalitz plots based on Equation 12. The B^- dominated areas are represented in blue, while B^+ dominated areas are red. It is not possible to comment on patterns of CP asymmetry in $B^{\pm} \to K^{\pm}K^{\mp}K^{\pm}$ based on Equation 12 as there isn't enough data points to show distinct features. However, this graph is in line with the results published by LHCb, and the features would likely emerge with additional data sets [20].
As mentioned in section 3, for CP violation to occur the numerator of Equation 6 must be non-zero. While the amplitude can slightly change based on the momentum [21], the weak phase does not vary for a specific decay. They only change based on the structure of a decay that takes place. Therefore they cannot be the cause for variance in CP violation localized on the Dalitz plot. Therefore only the strong phase contributes to variance in localized CP violation, which is a relationship that allows for an estimation of the strong phase based on the localized CP violation observed. As discussed in section 3, the strong phase of $B^{\pm} \to K^{\pm}K^{\mp}K^{\pm}$ decay proves to be highly challenging to describe from theoretical analysis, therefore experimental estimation is highly useful to determine the rate of this decay.

6 Conclusion

6.1 Aim

This project aimed to analyse the decay of the $B^{\pm}$ meson in the final state $K^{\pm}K^{\pm}K^{\mp}$ and to look for CP-symmetry violation that is consistent with the standard model. This asymmetry between matter and antimatter is crucial for understanding our matter-dominated universe.
Additionally, this project sought to improve our understanding of the dynamics involved in three-body decays. By studying the kinematic distributions of the final-state particles, we could better understand the strong interaction effects that contribute to CP violation.

6.2 Results

While the distribution of observed events B^+ and B^- was similar, the frequency of B^+ was higher. The calculation of the CP asymmetry parameter, done using the event frequencies, resulted in A_{CP}= -0.0379 ± 0.0099. This nonzero asymmetry indicates a 4% difference between the decay rates of matter vs antimatter. Which also falls in line with the LHCb results, whereas they found A_{CP} to be $-0.037 \pm 0.002 \pm 0.002 \pm 0.003$.

6.3 Implications

Although A_{CP} was found to be non-zero, as predicted, a difference of only 4% is not able to account for the domination of matter in the universe. The CP violation parameter is consistent with previous studies at LHCb [20]. It is multiple orders of magnitude too small than what is necessary to account for the observed imbalance. This implies yet-to-be-discovered physics, possibly extending the standard model. The obtained plot of the normalized difference between Dalitz plots provides a lead for estimating the strong phase in $B^{\pm} \to K^{\pm}K^{\pm}K^{\mp}$ decays. As the weak phase depends only on the decay occurring and amplitude only varies slightly with momentum, only the strong phase could influence this variance in asymmetry.

6.4 Limitations

One key consideration is the potential for particles to be misidentified as non-mesons due to inaccuracies or errors in detection by the LHCb detector. Such misclassification could result in erroneous rejection of an entry within the dataset, thereby affecting the reliability of the analysis. Additionally, the data selection process involved applying specific cuts, which, while necessary to refine the dataset, could introduce biases or inadvertently exclude relevant events.

One such data selection process included considering every particle that had a probability of at least 60% of being a kaon. However, this leaves a 40% probability of the observed particle not being a kaon.

Another limitation affecting the results arises from the inherent measurement errors in determining particle momentum. As discussed earlier in the theory section, momentum plays a crucial role in defining the boundaries of a Dalitz plot, which determines whether an event falls within the plot's valid region. Any inaccuracies in momentum measurement can lead to misclassification of events, including the incorrect inclusion, exclusion,

or misplacement of a specific event within the plot. Such errors may introduce distortions into the analysis, potentially impacting the interpretation of the results and the conclusions drawn from them.

These factors highlight the importance of exercising caution when interpreting the results and underscore the need for further validation and refinement in future studies.

6.5 Future directions

Building further upon the findings made during this project, there are several opportunities for future research to take place in order to help us understand better the CP-symmetry violation in B-meson decays. One potential direction we could take is the analysis of additional B-meson decay mechanisms involving different final-state particles, such as $B^+ \to \pi^+K^+K^-$ or $B^+ \to K^+\pi^+\pi^-$, to observe whether similar CP asymmetry patterns emerge across different decays. This would give an increased perspective on CP-violating effects and contribute or refute provided theoretical predictions.

Another promising direction for future work is the application of the ever-improving machine-learning techniques. This can be used to improve the discrimination of CP-violating effects in the Dalitz plot analysis. Models such as neural networks and boosted decision trees could be used to identify subtle asymmetry patterns that might not be detected with the traditional analysis methods.

Furthermore, an extension of the dataset used, to include more recent data from the LHCb, such as those from 2015-2018 and beyond, can allow for improved statistical precision and increased sensitivity to smaller CP asymmetries. We also want to mention the opportunity for upgrades made to LHCb, such as improved detector resolution, presenting an opportunity to revisit and even recreate this project with enhanced sensitivity. With a larger dataset, and more precise measurements, exciting findings such as rare intermediate resonance structures could be identified, which could lead to a better understanding of possible decay mechanisms.

By pursuing these opportunities for improvement, the study of CP-symmetry violation and B-meson decays can continue to play an important role in the understanding of the mechanisms which shape and govern the universe.

References

[1] LHCb Collaboration LHCb Experiment. *A typical LHCb event fully reconstructed during data taking on May 9th 2016. Particles identified as pions, kaon, etc. are shown in different colours.* May 2016. URL: https://cds.cern.ch/record/2151262.

[2] A. D. Dolgov. "CP violation in cosmology". In: *Reviews of Modern Physics* 71 (2 1999), S96–S104. DOI: 10.1103/RevModPhys.71.S96. URL: https://journals.aps.org/rmp/abstract/10.1103/RevModPhys.71.S96.

[3] Andrei D Sakharov. "Violation of CP invariance, C asymmetry, and baryon asymmetry of the universe". In: *Soviet Physics Uspekhi* 34.5 (May 1991), pp. 392–393. DOI: https://doi.org/10.1070/pu1991v034n05abeh002497.

[4] LHCb collaboration. *Matter Antimatter Differences (B Meson Decays to Three hadrons) - Data Files.* 2017. URL: https://opendata.cern.ch/record/4900.

[5] C Buchmüller W Lüdeling. *Field theory and the Standard Model.* Sept. 2006. URL: https://cds.cern.ch/record/984122/files/p1.pdf.

[6] David Griffiths. *Introduction to elementary particles.* John Wiley & Sons, 2008.

[7] Hans Nilles. *Gauge Theories and CP Symmetry.* Aug. 2018. URL: https://www.thp.uni-koeln.de/gravitation/100GT/nilles.pdf.

[8] Ashok Das and Thomas Ferbel. "Discrete Transformations". In: *Introduction to Nuclear and Particle Physics.* World Scientific, 2003. URL: https://archive.org/details/DasFerbelIntroductionToNuclearAndParticl page/n299/mode/2up?q=cpt&view=theater.

[9] Frank Wilczek. "The cosmic asymmetry between matter and antimatter". In: *Scientific American* 243.6 (1980), pp. 82–91.

[10] R.L. Workman. *2.1 Introduction.* 2022. URL: https://pdg.lbl.gov/2020/reviews/rpp2020-rev-ckm-matrix.pdf.

[11] Cecilia Jarlskog. "On Invariants of Quark and Lepton Mass Matrices in the Standard Model". In: *Comptes Rendus Physique* 13.2 (Jan. 2012), pp. 111–114. DOI: https://doi.org/10.1016/j.crhy.2011.09.008.

[12] Dhiman Chakraborty. *PHYS 684: Introduction to High Energy Physics.* Course webpage Accessed 17th January 2025. 2010. URL: https://nicadd.niu.edu/~dhiman/courses/phys684_10/.

[13] Ikaros I Bigi and A Ichiro Sanda. *CP violation.* Cambridge university press, 2009.

[14] Robert Fleischer. "CP violation in B decays: recent developments and future perspectives". In: *The European Physical Journal Special Topics* 233.2 (2024), pp. 391–408.

[15] Anthony Philip French. *Special relativity.* CRC Press, 2017.

[16] Thomas M Helliwell. *Special relativity.* University Science Books, 2010.

[17] J.D. Jackson. *Kinematics.* 2000. URL: https://pdg.lbl.gov/2016/reviews/rpp2016-rev-kinematics.pdf.

[18] L. Leśniak and P. Żenczykowski. "Dalitz-plot analysis of B±→K±K+K- decays". In: *Physical review. D/Physical review. D.* 110.3 (Aug. 2024). DOI: https://doi.org/10.1103/physrevd.110.033001.

[19] S. Navas et al. "Review of particle physics". In: *Phys. Rev. D* 110.3 (2024), p. 030001. DOI: 10.1103/PhysRevD.110.030001.

[20] R. Aaij et al. "Direct CP violation in charmless three-body decays of B± mesons". In: *Phys. Rev. D* 108.1 (2023), p. 012008. DOI: 10.1103/PhysRevD.108.012008. arXiv: 2206.07622 [hep-ex].

[21] A Abele et al. "Momentum dependence of the decay eta→pi+pi-pi0". In: *Physics Letters B* 417.1-2 (Jan. 1998), pp. 197–201. DOI: https://doi.org/10.1016/s0370-2693(97)01376-2.

A Python code

https://github.com/JennaHamers/B-KKK_Code/tree/0b3eda813b2e34611158aba7fd08f72db29085d0

B Contributions

Table 4: Contributions

Student	**Paper Contributions**
Oliver Brand	Introduction, Theory & Conclusion
Defne Adaş	Coding & Analysis, Results & Discussion
Jakub Gorzelany	Introduction, Theory, Methodology, Conclusion
Jenna Hamers	Coding & Analysis, Results & Discussion
Regina Ramirez	Abstract, Theory & Conclusion
Nelson van Rosmalen	Theory & Methodology
Finn Hamersma	Theory, Methodology, Results & Discussion